
Article:
Baillieu, A., Rahimov, E. and Marshall, M. orcid.org/0000-0003-3038-4626 (2025) The role of thermal properties in the wear mechanisms of an AlSi-polyester abradable. Wear, 562-563. 205618. ISSN 0043-1648

https://doi.org/10.1016/j.wear.2024.205618

Wear 562–563 (2025) 205618

Contents lists available at ScienceDirect

Wear

journal homepage: www.elsevier.com/locate/wear

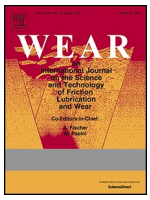

The role of thermal properties in the wear mechanisms of an AlSi-polyester abradable

Aaron Baillieu *, Eldar Rahimov, Matthew Marshall

Department of Mechanical Engineering, University of Sheffield, UK

ARTICLE INFO

Keywords:
Abradable testing
Wear testing
AlSi-Polyester
Metco 601
Adhesion
Thermal effects

ABSTRACT

During run-in and operation, the blades of a gas turbine engine may rub against the engine casing. To allow for these blade rubs an abradable coating is applied to the casing. However, the coating does not always cut smoothly, potentially wearing the blade. This paper focuses on the wear mechanics which occur with Metco 601, an AlSi-Polyester abradable which has been shown to produce a combination of blade wear and adhesion.

In this study, by testing AlSi-Polyester of different hardnesses at various incursion rates and blade speeds, it has been shown that there is a statistically significant difference in the wear behaviour observed at 0.02μm/pass compared with those observed between 0.2 and 2 μm/pass. Simultaneous recording of the blade front, thermal hotspots on the blade and abradable, and force measurements have been used to relate observed wear mechanics to the thermal behaviour of the abradable. Results showed that at incursion rates above 0.2μm/pass high force application rates lead to localised hotspots on the abradable and sporadic adhesion events. At 0.02μm/pass the force application rate, and hence thermal energy flux into the abradable, is more gradual, allowing heat to spread across the abradable surface. The more uniform abradable temperature leads to large areas of simultaneous wear, demonstrating how the abradables ability to manage the thermal energy can have a significant impact on its wear performance. This has been further verified through the observation of a reduction in abradable temperature as the test progresses which aligns with a reduction in the thermal resistance through the abradable and also an observed transition from adhesion to blade wear.

This work has shown that the management of thermal energy within AlSi-Polyester has a significant impact on the observed wear mechanisms, improving the understanding of why the wear mechanics vary with incursion rate.

1. Introduction

AlSi-Polyester is an abradable coating typically found within the low-pressure compressor of a gas turbine, protecting the tips of the blades in the event of a rub with the casing. A common example of this material is Metco 601, formed of an Aluminium (balance) Silicone (7 %) (AlSi) bulk with a Polyester filler (40 %), M601 is designed to be safe to use with Titanium Blades [1] but, in reality, the rub conditions can lead to significant variability in the abradable cutting performance.

Work by Borel et al. on AlSi-Polymer Abradables found that the incursion rate was a significant factor in determining the performance of the abradable. With an Aluminium-Polyester abradable the primary wear mechanisms observed were adhesive wear and blade melting, with adhesions being more prevalent at the higher incursion rates [2].

Alongside the increasing rate of adhesions, Watson et al. showed a trend of increasing forces with increasing incursion rates from 0.2 to 2 μm per pass of the blade [3], this aligns with well-established laws of adhesive wear put forward by Archard, stating that the volume of adhesive wear is proportional to the normal load [4]. However, this relationship did not hold at the lower incursion rate of 0.02μm/pass.

The predictable wear performance between 0.2 and 2 μm/pass is beneficial for engine manufacturers as the initial run-in of the engine is completed in controlled conditions, allowing for some control over the incursion rates which will be witnessed by the abradable liner. However, during operation, tip – liner contacts mostly occur due to external factors such as turbulence. These conditions are more likely to produce incursion rates which are in the order of 0.02μm/pass. Testing has shown that at these incursion rates significant amounts of blade damage and abradable scoring occurs [2,3]. Within the engine the increased tip clearance, and scored abradable profile, leads to efficiency loses as

* Corresponding author. E201-20, 3 Portobello St, Engineering Heartspace, The University of Sheffield, S1 4DT, UK.
E-mail address: ajbaillieu1@sheffield.ac.uk (A. Baillieu).

https://doi.org/10.1016/j.wear.2024.205618
Received 13 May 2024; Received in revised form 30 September 2024; Accepted 31 October 2024
Available online 20 November 2024

turbulent air is able to flow around the blades. The uncertainty around the wear behaviour of AlSi-Polyester at lower incursion rates is therefore a significant issue for engine manufacturers, and hence has been a key area of focus for abradable research.

Watson et al. showed that, although adhesion rates fell, the peak forces present at 0.02μm/pass did not differ significantly to those seen at 0.2 μm/pass [3]. Beyond this the forces and temperatures observed during the test followed a cyclic pattern, something unique to tests at these low incursion rates.

The impact of material temperature on the rate of adhesive wear is not included in the original relationship proposed by Archard [4]. However, recent work by Gåård et al. has shown that severe adhesive wear can occur more readily at increased temperatures [5], with this result aligning with Atomic Force Measurements which show adhesive forces at the atomic level increasing with temperature for titanium, stainless steel and low alloyed steel [6].

A link between temperature and adhesive wear during an abradable rub event was subsequently observed by Baillieu et al. who observed adhesion events on the blade aligning with hotspots on the abradable [7]. However, this study did not provide a sufficient range of data to determine the nature of the relationship. Looking to understand the relationship further it is important to understand how energy within a rub is dissipated. Experimental and analytical work by Agrapart et al. has shown that during a rub event between a titanium blade and an AlSi-Polyester abradable most of the energy of the rub is dissipated as heat, with a heat partition ratio of 95 % in the abradable coating and 5 % in the blade [8]. With a large proportion of the heat flowing into the abradable, its ability to manage this energy will have a significant impact on the temperature of the rub event.

Considering the nature of the heat transfer further, work looking into the thermal properties of AlSi-Polyester by Bolot et al. has shown that the microstructure of the abradable has a significant bearing on its thermal properties. AlSi-Polyester coatings are manufactured using a plasma spray process, this results in a bulk of AlSi with clumps polyester dispersed throughout. During the spray process voids can form within the substructure, this results in a microstructure such as that shown in Fig. 1. When there is a thermal gradient across the abradable the majority of the heat flow follows connected chains of AlSi [9]. As the hardness of a sample reduces, the ratio of voids and polyester to AlSi increases, which breaks up the connected chains of AlSi and therefore reduces thermal conductivity of the sample. Watson et al. was in turn able to develop this work further, showing how the inherent randomness of the plasma spray manufacture process used for Metco 601 leads to significant variation in thermal properties at different locations within a single sample [10].

Building on these studies, this study looks to apply the in-situ measurement techniques developed by Rahimov et al. [11] to relate measured adhesion volumes with forces and rub lengths for a range of different test conditions to identify any deviations from Archard's relationship. The in-situ thermal measurement techniques developed by Baillieu et al. will then be applied to develop an understanding of why these deviations occur [7].

2. Method

The data for this study was collected on a pair of spindle test rigs situated at the University of Sheffield. These rigs use a spindle motor to spin a disk with a Titanium (Ti-6Al-4V) test blade (Fig. 2a) up to a desired blade tip speed. When the desired tip speed is reached a 3 mm thick Metco 601 sample (Fig. 2b) is pushed into the path of the blade using a motorised stage, its speed can be varied to adjust the incursion rate of the test. The majority of the data for this study was collected using a High-Speed Rig (Fig. 3) which is able to reach blade tip speeds of 280 ms^{-1} [11], this rig was used to allow for the largest range of test conditions when looking for patterns in wear behaviour. However, when using in-situ thermal measurement techniques a Low-Speed Rig (Fig. 4) must be used. This rig tests the same blade and abradable samples but makes use of a smaller disk and less powerful motor, limiting blade tip speeds to 200 ms^{-1} [12]. The reduced risk in testing with the Low-Speed rig allows for a simplified enclosure which can facilitate a high frame rate thermal camera.

Although these rigs make use of different sized disks both have been able to produce similar, engine representative, wear results. With Rahimov comparing test results between the two rigs to show that at any given test condition a similar output is obtained from each [13].

The AlSi-Polyester samples used in this work were created by an atmospheric plasma spray process using a Oerlikon Metco plasma spray gun. They were sprayed onto a 2 mm thick A2 Stainless Steel backing plate prepared following the surface preparation guidelines provided by Oerlikon Metco. The hardness of the abradable can be varied by adjusting spray parameters such as powder flow rate, the current, and the distance between the gun and the backing plate [14]. From each batch an abradable sample was tested against the Rockwell 15Y scale to validate that the coating is of the desired hardness.

A harder sample of AlSi-Polyester has a higher proportion of the larger AlSi particles than voids or polyester. However, due to the higher temperatures and particle velocities involved in the spray process of harder samples the particles typically become more compacted on contact with the backing plate. Due to this there is no clear trend between the hardness and the roughness of the samples. The samples used in this work all had Sa values between 25 and 35 μm (Measured to ISO 11562, applying a linear planar, order 0 roughness filter in accordance with ISO 16610-61).

Both rigs are able to measure the forces acting on the abradable during the rub through the use of Kistler tri-axial piezoelectric force transducers fitted below the abradable sample. Both rigs are also fitted with a camera aimed at the leading edge of the blade. Through the use of stroboscopic imaging footage from this camera can be used to observe how the blade changes during a rub.

This footage, using the methods developed by Rahimov et al. [11], can then be aligned temporally with the normal and tangential forces.

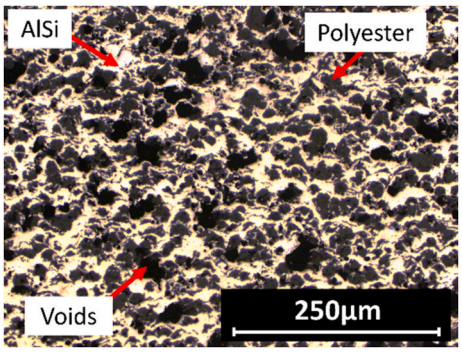

Fig. 1. Metco 601 microstructure.

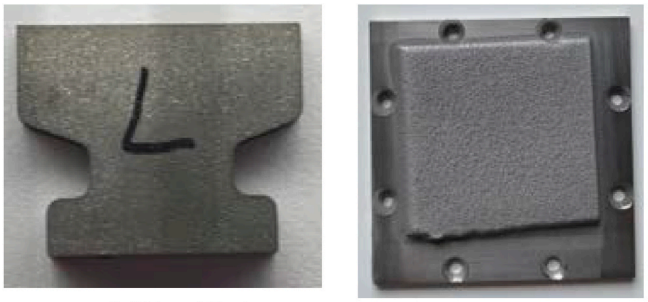

Fig. 2. Blade and abradable samples [7].

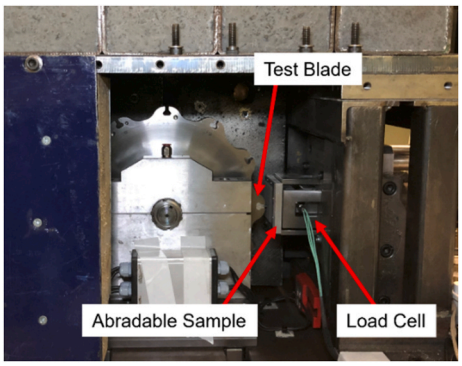

Fig. 3. High Speed Spindle Test Rig [13].

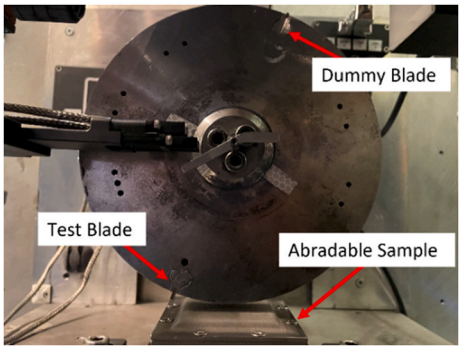

Fig. 4. Low speed spindle test rig.

From the images of the leading edge Rahimov et al. were able to extract the profile of the blade, mapping how the blade profile changes for the duration of the test. Although it is not possible with this test setup to measure the profile of the abradable during the rub, Rahimov et al. [11] has shown that the profile of the abradable is the inverse of the highest points on the blade during the test. Measurement of just the blade alone is therefore sufficient to get a good view of the wear mechanisms occurring during the blade/abradable contact.

As this work is looking to relate back to the relationships put forward by Archard [4] the key characteristics which must be extracted are the volume of adhesive wear which occurs during the rub, the rub length during which adhesions formed, and the normal force during that process. As adhesions form and break off for the duration of the rub this cannot be measured post-test, instead is calculated from the in-situ blade profile measurements.

2.1. Wear volume

To calculate adhesion volume, in-situ images of the front of the blade are used. For each image the blade edge is detected, and the total area enclosed by that edge is measured and multiplied by the blade depth to calculate volume, the volume of the previous frame is then removed. This gives the change in volume of the blade between each image.

This wear volume is over a blade with a width of 20 mm, which is the standard size used within the test rigs used by Rahimov et al. [11] and Baillieu et al. [7]. However, as can be seen in Fig. 5, lighting gradients for some tests produced dark regions in the centre of the blade, reducing edge detection accuracy. To overcome this, tests with uneven backgrounds had 3 mm from the centre of the blade excluded from the analysis. To ensure that the wear volumes for all tests are directly comparable, volumes for tests with the centres cropped have been multiplied by the width ratio of a full blade to a cropped blade. This means that all wear volumes used in this work here are mm^3 over a 20 mm width.

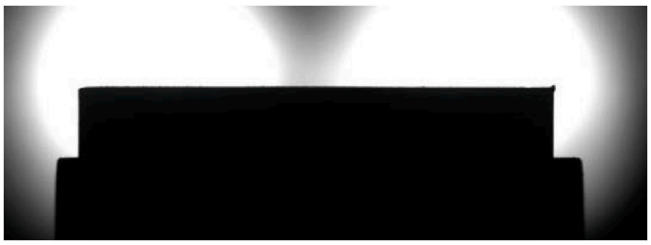

Fig. 5. Uneven illumination of blade.

To validate the accuracy and reliability of the blade profiles extracted from the stroboscopic images, the final blade profile extracted was compared with a profile map of the post-test blade captured with a Bruker Alicona InfinteFocusSL. An example of the results of this are shown in Fig. 6, with Fig. 6b showing the detected edge aligning with the profile from the Alicona. This process was repeated for each test batch to ensure that no errors were introduced into the stroboscopic system during setup.

2.2. Rub length

The rub length through the duration of the test does not vary linearly, this is due to the blade cutting a curved path into a flat abradable sample. In order to calculate the rub length which has occurred between two images the total rub length (L, m) at each image must be calculated from the current incursion depth (i, m), incursion rate (r, m/pass) and the disk radius (R, m).

From the current incursion depth, the number of passes which have occurred (N) can be calculated using $N = i/r$. Using this value Equation 1, derived by Rahimov et al. [11], can be used. The rub length per image is therefore the difference in total rub length calculated between two frames.

$$L = \sum_{n=1}^{N} 2R\cos^{-1}\left(\frac{R - in}{R}\right)$$

Equation 1 – Calculation of total rub length.

2.3. Normal force

The capture rate from the load cell mounted beneath the abradable sample (100 kHz) is much higher than the frame rate of the camera (30 Hz). To extract the normal force which was present for each image the

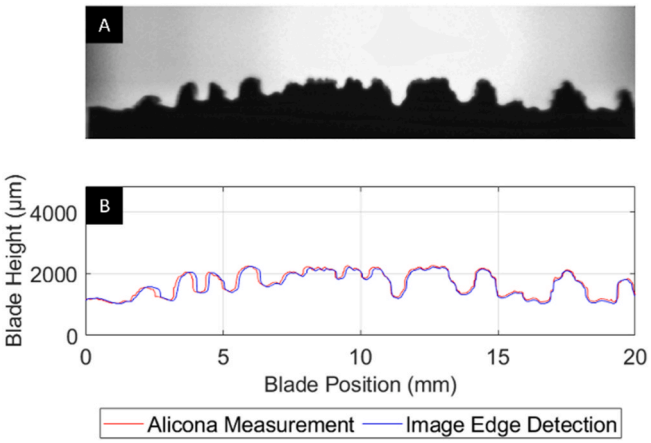

Fig. 6. Blade profile measurements from a test at 200 m/s on a 77.5HR15y sample **A** - The stroboscopic image of the blade. **B** – Comparison of edge detection to Alicona profile measurements.

mean force is calculated between the current and previous frame.

When the wear volumes, rub lengths, and forces have been extracted for each image the frames which include adhesive wear can be isolated by removing any frames with a wear volume change $\leq 0\ mm^3$. The rub lengths and adhesion volumes can then be summed to give a total volume of adhesion and total rub length, similarly the force values can then be averaged to calculate the average normal force while adhesions were forming.

By running tests with AlSi-Polyester samples of varying hardness, at varying speeds and incursion rates we know from previous work by Borel et al. [2] and Watson et al. [3] that the volume of adhesions which will form on the blade will vary. With the additional information we are able to extract from the in-situ measurement techniques, the volume of adhesion can be measured and related back to the relationship proposed by Archard [4]. An overview of the tests completed for this study are detailed in Table 1. This table breaks down the completed tests into a matrix showing, for every combination of incursion rate and hardness, how many tests were completed at each tip speed (for example '1 × 280' = 1 test at 280 ms^{-1}). Tests performed on the Low-Speed rig with the addition of the thermal camera are also noted.

It is expected from work by Watson et al. [10] that the data collected at 0.02μm/pass will follow a different pattern to the data collected at higher incursion rates. To investigate these tests further the in-situ thermal analysis techniques developed by Baillieu et al. [7] will be employed for a range of incursion rates. These techniques make use of a high frame rate FLIR thermal camera aimed at the abradable at a shallow angle to ensure the view is not obstructed by the disk. This camera is triggered by a light gate which is positioned such that the blade obstructs the view of the abradable every other frame. These frames can then be split into images of just the blade and just the abradable in post processing. The abradable images are also warped using homography methods to allow the abradable hotspots to be aligned with blade hotspots and adhesion formation.

Using these tools, it is possible to look at individual points on the abradable and to observe how the temperature varies during the test. It is also possible to identify individual adhesion events on the blade and extract the temperature of the abradable and the blade at this location.

By applying these tools to tests completed at a range of different incursion rates it will be possible to observe how the blade and abradable temperatures differ at different test conditions.

3. Results

The initial rub maps produced by testing samples of AlSi-Polyester of the same hardness and speed but with different incursion rates align well with the results presented by Borel et al. [2]. For example, at a blade tip speed of 100 m/s and an abradable hardness of 69HR15y, Fig. 7 shows high levels of adhesion at 2 μm/pass with the volume of adhesions reducing at lower incursion rates. At 0.02μm/pass there is a significant amount of blade damage.

Table 1
Test matrix.

		Hardness (HR15y)		
		Low (53.5–55.0)	Medium (60.5–68.6)	High (70.0–77.5)
Incursion Rate (μm/pass)	0.02	1 × 100	1 × 100	1 × 100
		1 × 200	1 × 200	1 × 200
		1 × 280	1 × 280	1 × 280
		1 × 200[a]		1 × 200[a]
	0.20	1 × 100	1 × 100	1 × 100
		1 × 200	1 × 200	1 × 200
		1 × 280	1 × 280	1 × 280
				1 × 200[a]
	1.00	1 × 100[a]	1 × 100[a]	1 × 100[a]
		1 × 200[a]	1 × 200[a]	1 × 200[a]
	2.00	1 × 100	1 × 100	1 × 100
		1 × 200	1 × 200	1 × 200
		1 × 280	1 × 280	1 × 280
				1 × 200[a]

[a] Data collected on the Low-Speed Rig.

Using the in-situ data analysis methods described above, each test had been analysed and the results have been plotted in Fig. 8. The results have been plotted in a manner which relates to Archard's relationship (Equation 2). This relationship states that the ratio of adhesion volume (A) to rub length (l) should be proportional to the ratio of normal force (F) to hardness (H).

$$\frac{A}{l} \propto \frac{F}{H}$$

Equation 2 – Archard's Relationship

Between 0.2 and 2 μm/pass a line of best fit can be plotted with a Pearson correlation coefficient of 0.80, showing that there is a strong relationship between adhesion rate and the force to hardness ratio, aligning with Archard's relationship. This plot also shows how the spread of data increases with increasing incursion rate, which is due to the reduced test time at higher incursion rates limiting how much data can be collected. However, even with the increased spread at the higher incursion rates the mean value for each incursion rate sits on the line.

If this relationship were to hold at 0.02μm/pass the mean value of the 0.02μm/pass data would also sit on the line. To test this a single sample T-Test has can be completed with the null hypothesis that the mean of the residuals from the 0.02μm/pass data about the linear relationship is zero. With a sample mean of −0.140, a sample standard deviation of 0.031, and 10 degrees of freedom it is possible to reject this null hypothesis at a confidence level of 99 %. This shows that there is a statistically significant difference between the mean at 0.02μm/pass and the linear relationship.

While Fig. 8 shows the deviation from the linear relationship at a global level, these differences can also be seen when directly comparing data from individual tests. For example, Fig. 9 shows how adhesion formation varies between three 0.02μm/pass tests at 100 m/s with varying hardnesses. The ratio of average normal force to hardness for each of these tests remained consistent at 2.07 ± 0.16 N/HR15y, and therefore from Archard's relationship the adhesion rates are also expected to remain consistent. However, it can be seen that as the hardness reduces adhesion formation becomes more favourable.

These results show that, although existing relationships are able to make reliable predictions for the volume of adhesions expected at high incursion rates, at low incursion rates there are additional factors at play which influence adhesion formation with AlSi-Polyester.

To determine what these factors could be, differences between the different incursion rate tests can be investigated from the in-situ data collected.

A significant difference between the different incursion rates is the duration of the tests, and the rate at which the normal load increases. The time duration for each test is proportional to the incursion rate. For 2 and 0.2 μm/pass a 2000 μm incursion at 200 m/s lasts for 3s and 30s respectively whereas a 0.02μm/pass incursion will last for 300s (5 min). With the increased test length, while the peak and average forces experienced at 0.2 and 0.02μm/pass may be similar, the rate of increase in force is lower at the lower incursion rate. An example of this is shown in Fig. 10, which shows the first 3.5 s of 200 m/s tests of abradable samples with a hardness of 77.5HR15y at varying incursion rates.

Further differences are visible in the thermal camera footage showing how the abradable surface heats up. For example, Fig. 11 shows snapshots of the blade front and the abradable temperature for two 200 m/s tests on 77.5HR15y samples. Each snapshot is selected at a time when there are hot spots visible on the abradable surface. Fig. 11a, b shows how at 0.2 μm/pass hotspots occur at isolated regions on the abradable at positions which align with adhesion formations on the

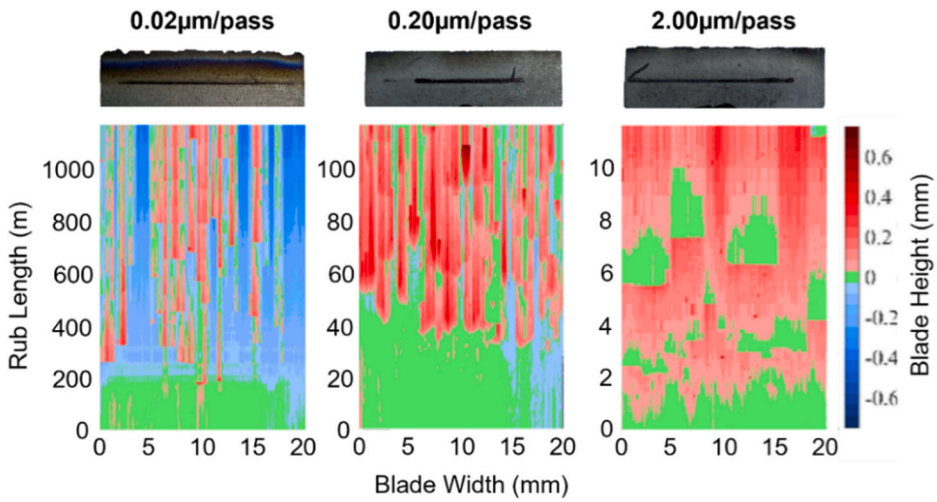

Fig. 7. Rub maps at different adhesion rates for abradables of the hardness 69HR15y at a tip speed of 100 m/s.

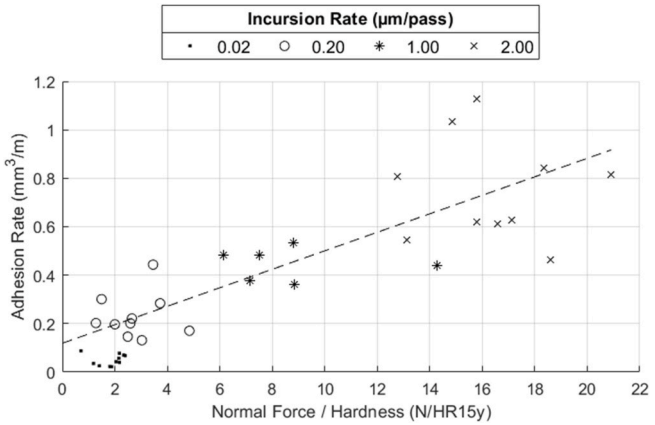

Fig. 8. Adhesion rates against force/hardness.

blade. At 0.02µm/pass Fig. 11c, d shows how the blade heats up more uniformly with adhesions being distributed evenly along the blade edge.

This more even wear distribution leads to periodic drops in contact area as large-scale fracture events occur. This explains the cyclic force behaviour observed by Watson et al. [3]. The cyclic behaviour is also observed in the blade and abradable temperatures, an example of this is shown in Fig. 12 for a 200 m/s rub at 65.8HR15y. This figure shows the blade temperature, abradable temperature and blade height at a single location on the blade for a 0.02µm/pass test. From this plot the temperature peaks can be seen to align with wear events, but what can also be observed is the transition from adhesion formation and fracture events early in the rub, to blade wear as the rub progresses.

A piece of work which helps to draw these observations together was completed by Watson et al. [10] which showed how reducing the hardness of AlSi-Polyester also led to a reduction in its thermal conductivity, highlighting a potential link between adhesion rate and thermal management within the abradable.

Considering first the overall difference in heating seen between high and low incursion rates, it is notable that at different incursion rates there is also a difference in the thermal input into the abradable during the rub. Larger incursions lead to larger flash temperatures [15], and the more gradual increase in normal force at 0.02µm/pass leads to a gentler increase in the rate of frictional heating [16]. The combination of differing thermal input and the ability of the abradable to manage that heat can explain the differences observed with the thermal camera.

At higher incursion rates with high rates of frictional heating the irregularity of the thermal properties within a single abradable (as shown by Watson et al. [10]) lead to local hotspots, and localised wear events. At 0.02µm/pass the heat flow rate is lower allowing the heat to flow throughout the surface, this makes the heating less dependent on irregularities within the abradable and allows for an increase in the

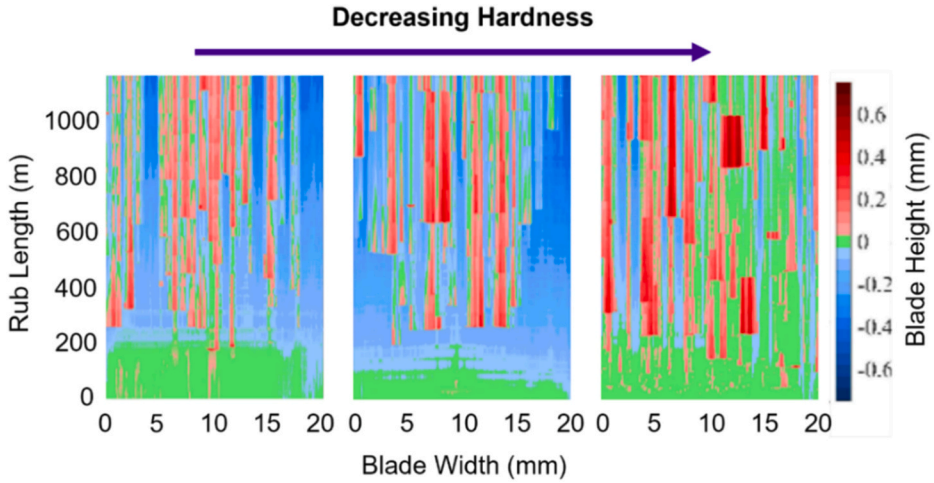

Fig. 9. Rub Maps for 0.02µm/pass tests with decreasing hardness at a tip speed of 100 m/s.

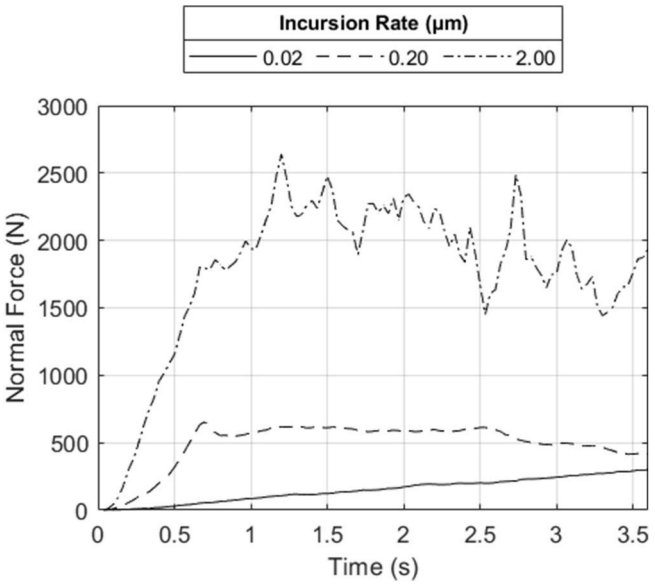

Fig. 10. Force application rate at varying incursion rates for samples of hardness 77.5HR15y at 200 m/s.

abradable bulk temperature. At these test conditions the further differences between the wear behaviours observed at different abradable hardnesses highlight the abradables ability to manage this heat as a potential factor determining its wear performance.

Moving to the transition from adhesion to blade wear seen at lower incursion rates, if the temperature of the abradable is a significant factor in the formation of adhesions, with higher temperatures being more favourable to adhesion formation, a reduction in surface temperature would be expected as the rub progresses in order to explain the transition from adhesion formation to blade wear shown in Fig. 12. To better understand how the abradable manages heat, and how that varies throughout a rub, a thermal model can be used.

4. Thermal model

To go beyond the surface and investigate the heat flowing through the abradable a simplified thermal model was created using the PDE Toolkit within MATLAB [17]. This model took the form of a 2D cross section of the abradable with a circular arc removed with a radius equal to the disk of the low-speed spindle test rig used in this study, this was created within the PDE Toolkit using the *geometryFromEdges* function. Thermal properties of the abradable were set to those measured by Watson et al. [10] and assumed isotropic. This model is able to run steady state and transient analysis using the *createpde("thermal", "steadystate")* and *createpde("thermal", "transient")* functions respectively. This allows for visibility of how heat flows through the abradable to the backplate (Fig. 13).

A transient analysis with this model highlights the importance of test duration to thermal management within the abradable. Fig. 14 shows how the temperature at the abradable surface compares to the temperature at the backing plate of the sample. The analysis was completed for a 3 mm thick sample with an incursion depth of 500 μm, applying a constant heat flux of 1 W to the rub surface. Due to the poor thermal diffusivity of AlSi-Polyester (2670 m^2/s for 55HR15Y [10]) the time required to reach a steady state thermal condition across the abradable is large compared with the durations of the 2 and 0.2 μm/pass tests. These results align well with the observations that show during the longer duration tests thermal energy was able to spread across the surface, while for the shorter tests hotspots were more localised as there was insufficient time for the heat to spread before wear occurred.

However, these results also point to a difference in the effectiveness of thermal conductivity as a mechanism for thermal energy removal from the abradable via the back plate. At 0.02μm/pass the temperature distribution across the abradable will be near steady state and therefore heat flux through the abradable will be at its maximum. For 0.2 and 2 μm/pass tests the temperature across the abradable will be transient and therefore there will be a lower heat flux through the backplate while more energy is being stored within the abradable.

For a test with a 200 m/s blade speed, a 2 μm/pass test will produce a 0.66 mm incursion in 1 s and a 0.2 μm/pass test would produce a 0.066 mm incursion. The abradable material removed will either adhere to the blade or will come away as chips, taking with it any thermal energy

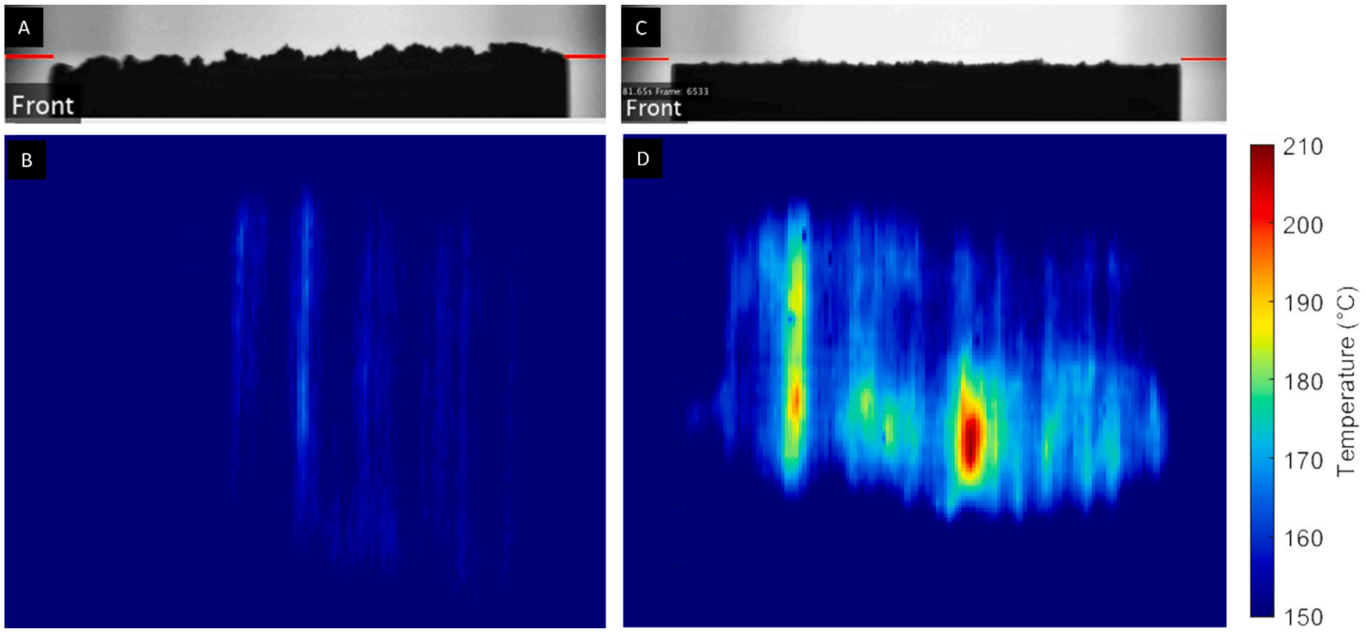

Fig. 11. Snapshots showing hotspots from tests at 200 m/s of 77.5HR15y samples. **A** – The blade front at 0.2 μm/pass. **B** – The abradable temperature at 0.2 μm/pass. **C** – The blade front at 0.02μm/pass. **D** – The abradable temperature at 0.02μm/pass.

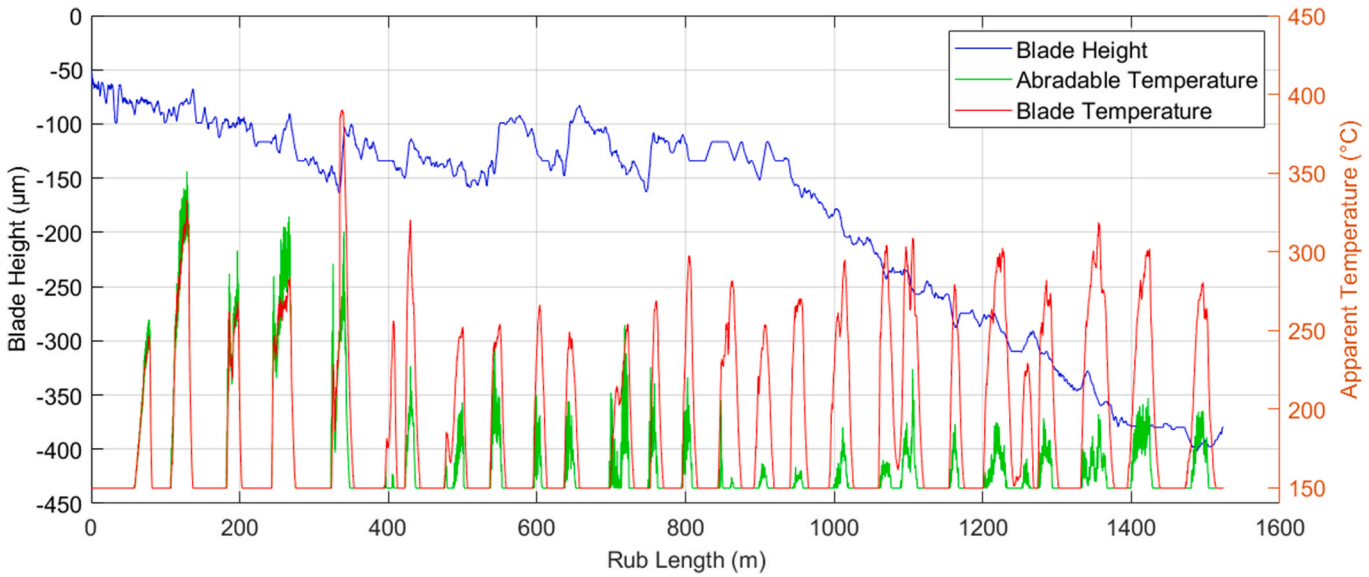

Fig. 12. Blade and abradable temperatures alongside blade height at a single point on the blade for a 0.02µm/pass test at 200 m/s, 65.8HR15y.

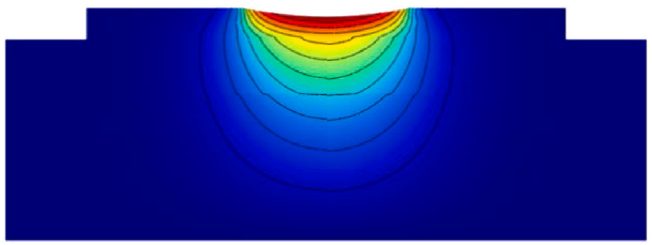

Fig. 13. Thermal model of abradable.

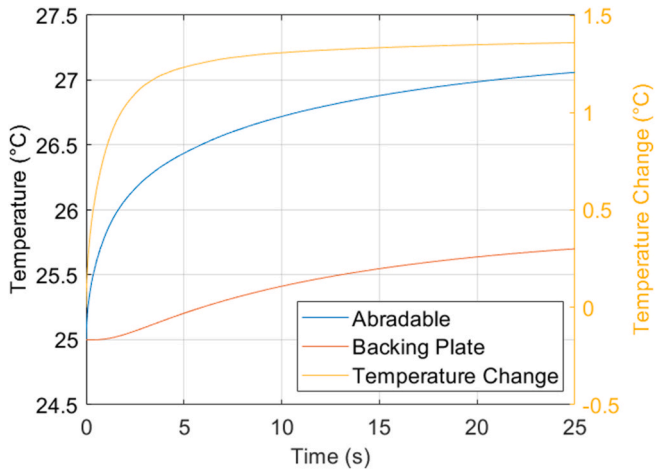

Fig. 14. Transient Analysis of temperature distribution across abradable for a 1 W thermal load at a 500 µm incursion.

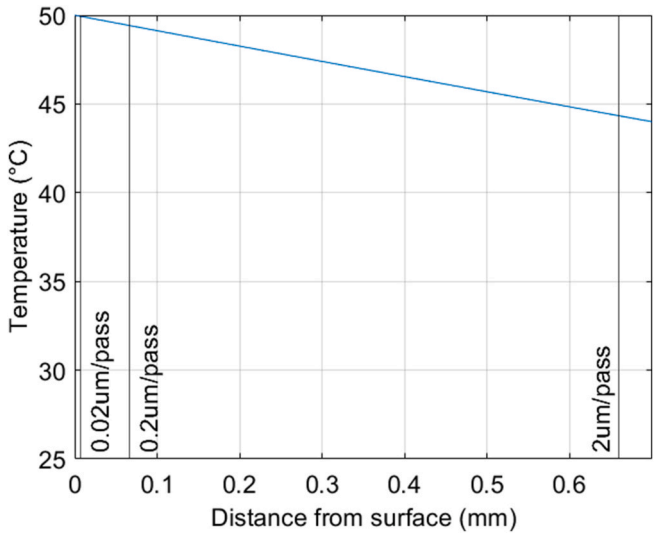

Fig. 15. Temperature distribution through abradable 1s after a 50 °C thermal load is applied.

stored within it. Fig. 15 shows the simulated heat distribution through the abradable after 1s of applying a thermal load of 50 °C to the rub surface with a 25 °C starting temperature. The vertical lines in this plot show how much material is removed in that same time period at each incursion rate. At 2 µm/pass it can be seen that a significant amount of high temperature material is removed, removing energy from the system, and revealing a layer of lower temperature abradable. Conversely, at 0.2 µm/pass some high temperature material is removed, but the effect is not as significant as volumes are more reserved. At 0.02µm/pass only 0.0066 mm of material is removed per second, and at these rates the material revealed after the removal is of similar temperature to the previous layer, and therefore thermal energy removed through material removal is far less effective at these lower incursion rates.

This analysis suggests that the primary mechanisms for removing thermal energy differ between high and low incursion rate tests. At incursion rates higher than 0.2 µm/pass the energy removal through conduction is limited as the temperature distribution within the abradable is still transient. However, there is a high rate of material removal from the abradable, taking heat away through chips. At 0.02µm/pass the rate of material removal is far lower and therefore less energy is removed from the system through this mechanism. Instead, the large timescales for this test lead to a near steady state temperature distribution through the abradable and therefore maximise conductive heat transfer out of the backplate.

If conduction through the abradable is a leading mechanism for thermal energy removal during a 0.02µm/pass test, it would be expected that temperature of the abradable surface would reduce as the test continues. This is because, as shown in Fig. 16, the thickness of the

abradable reduces as the test progresses, the length of the rub track also increases. The increase in surface area and reduction in thickness will lead to a reduction in thermal resistance through the abradable. In Fig. 16, r is the radius of the circular path taken by the test blade, d is the incursion depth, and t is the initial thickness of the abradable sample.

The change in thermal resistance as the test progresses can be extracted from the thermal model using a quasi-steady analysis with 1 W of heat flux being applied to the rub surface. The temperature difference between the rub surface and the backplate is the thermal resistance of the abradable. To validate the model an analytical solution can be derived from the simplified geometry shown in Fig. 16. This geometry can be broken up into a series of vertical rectangles of width dx and height equal to the thickness of the abradable at that location. By treating these rectangles as a series of parallel thermal resistors, each with a thermal conductivity of k and a depth W, it is possible to integrate along the rub length to find the total resistance of the abradable. The integral to do this is shown in Equation 3, with limits (lim) being calculated as the width of the abradable under the rub track.

$$1 \Big/ R = kW \int_{-lim}^{lim} \frac{1}{r - d + t - \sqrt{r^2 - x^2}} dx$$

$$lim = \pm \sqrt{d(2r - d)}$$

Equation 3 - Analytical solution for Thermal resistance

The results of the simulation and analytical solution are shown in Fig. 17. Both solutions predict similar thermal resistances through the abradable, with the rate of change in resistance reducing as the test goes on. This is expected as the rate of increase in rub length is not linear.

Finally, it should be noted that the analytical solution predicts a larger resistance than the model, this is because the simplified geometry only includes the material directly below the rub whereas the computational model includes the entire abradable at all rub depths.

5. Discussion

The experimental results can be combined with those from the thermal model to further understand the wear mechanisms present.

Taking the temperature at a point on the abradable from the 0.02μm/pass test shown in Fig. 12 and extracting only the peak values of the blade and abradable temperature the trend in temperature with rub depth can be seen (Fig. 18). While the blade temperature remains fairly constant throughout the rub, the abradable temperature reduces as the rub progresses, with a pattern which mimics that predicted in the analysis in Fig. 17.

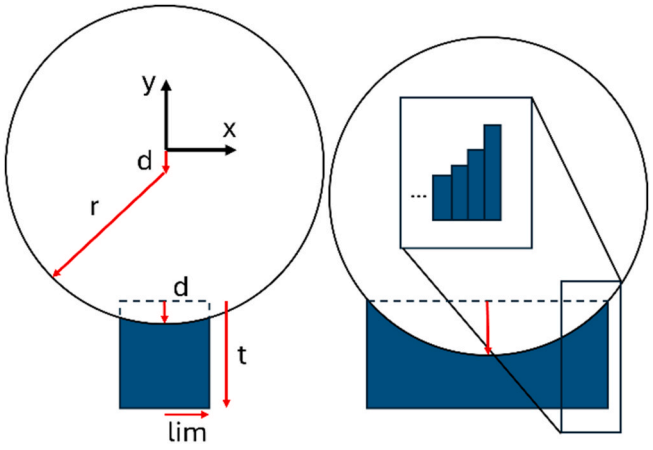

Fig. 16. Simplified abradable geometry.

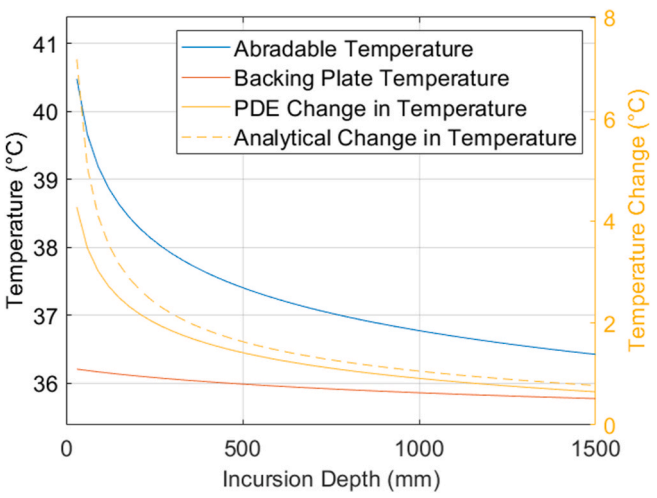

Fig. 17. Predicted thermal resistance of the Abradable at varying incursion depths.

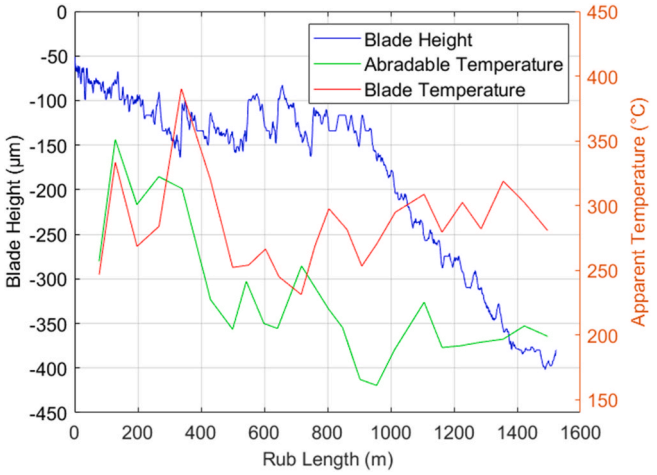

Fig. 18. Peak blade and abradable temperatures from the data shown in Fig. 11 alongside blade height.

These results align with the theory that at the lower incursion rates conduction is a leading mechanism for thermal energy removal, and as the rub progresses the abradable becomes better at conducting heat to the backplate, reducing the surface temperature.

Evidence in support of this conclusion can also be found by comparing individual heating cycles from the beginning of a rub and from the end of the rub. Fig. 19a shows an enlarged view of three heating cycles taken early in the rub, during a period where adhesions were forming readily on the blade. Looking at the time phasing of the blade and the abradable heating it can be seen that both bodies heat up at similar rates and times, and also that the adhesion formation on the blade aligns with the peaks in the abradable temperature.

Fig. 19b shows the same data but taken towards the end of the rub. For these thermal cycles the rate of heating of the blade remains similar to what was observed early in the test. However, the rate of heating of the abradable is noticeably less. At this stage in the test there are fewer adhesions forming and instead the blade is wearing, with the wear events aligning with the peaks in blade temperature.

As the peaks in blade temperature do not show a significant reduction during the rub, but there is a clear transition from adhesions to blade wear, these results also show how the adhesions act as a sacrificial layer during the early stages of the test. This is evident in Fig. 19a where the blade length is seen to increase at abradable hotspots before

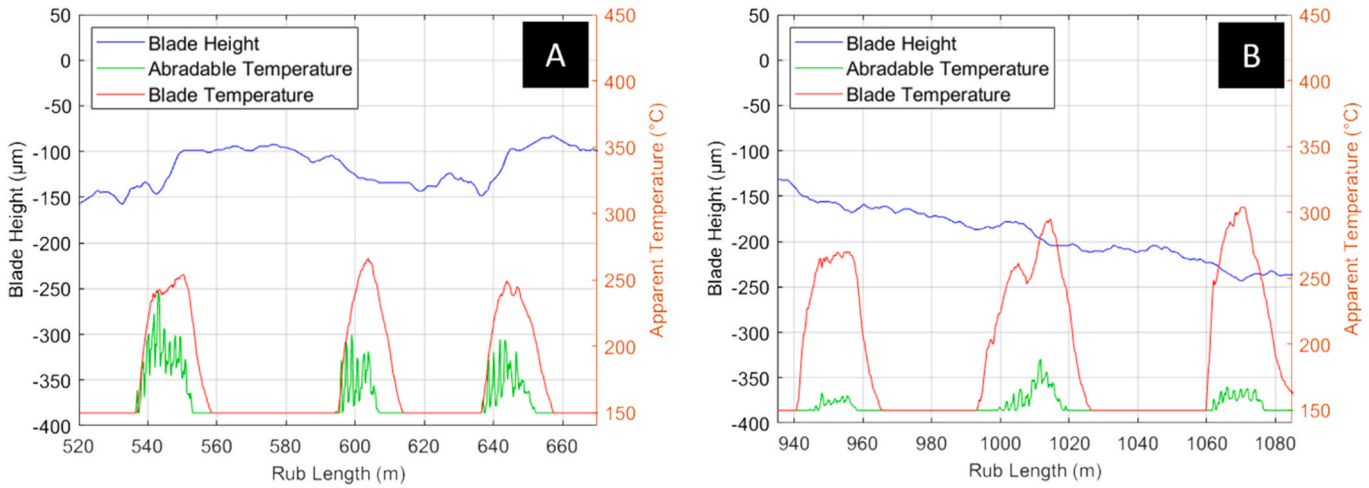

Fig. 19. Plots from a 0.02µm/pass test showing the abradable and blade temperatures alongside blade height from three cycles extracting from **A** – early in the rub **B** – Late in the rub.

subsequently reducing again at blade hotspots. As the test continues the abradable temperature does not increase as rapidly and the blade wears before adhesions are able to form.

With the application of these results an explanation can now be put forward to answer why the wear behaviour of AlSi-Polyester at 0.02µm/pass differs from that of higher incursion rates, and why the force response exhibits a unique cyclic profile.

At high incursion rates local hotspots due to the high frictional heating produce sporadic adhesion events. At the lower incursion rates the lower force application rate produces a smaller heat flux over a larger time period, allowing the heat to dissipate more uniformly across the surface. The more uniform surface temperature leads to an even distribution of wear events over the surface, and hence periodic large-scale adhesion and fracture events are established which lead to a significant reduction in contact area, and hence load. These periods of reduced loading also allow for the abradable to cool. This cooling, along with the improved thermal conductivity through the abradable, allows for lower bulk temperatures and hence leads to a shift from a primarily adhesive wear mechanism to one of blade wear. This agrees with work by Gåård et al. [5,6] which show that adhesive wear is more prevalent at increased bulk temperatures. These theories are further supported by a transition from adhesion formation to blade wear which aligns with a reduction in abradable surface temperature.

These additional insights into how the bulk temperature of the abradable can impact the adhesion rates of AlSi-Polyester provide an additional tool to engine manufactures when trying to produce more predictable operational wear conditions. However, they also highlight a significant difference between the tests completed here and the real-world applications.

In operation AlSi-Polyester will typically be found in the low-pressure compressor of the engine. Although this is one of the cooler parts of the engine, temperatures can be in the region of 300 °C. The impact on the abradable is elevated further by the fact that the casing can also be at similar temperatures. With the high temperature of the abradable and casing the abradable will not be able to dissipate heat from the rub as readily, in fact the abradable will be held at temperatures which have been observed during adhesion formations in testing. This could make AlSi-Polyester applied to a real engine far more susceptible to adhesive wear than when testing in a test rig. This deviation from a real-world application could be compensated for through the use of heating plates fitted under the abradable. By applying heat to the abradable backing, it will be possible to better control the heat flux through the abradable during a test. With this additional control it would be possible to extract a more detailed relationship between temperature, force and adhesion rates, providing engine designers with tools which will allow them to better predict the wear behaviour of AlSi-Polyester within an engine.

6. Conclusion

At incursion rates higher than 0.2 µm/pass the wear performance of Metco 601 follows Archard's relationship [4]. At 0.02µm/pass wear mechanisms are harder to predict with fewer adhesions and more blade wear being observed, even though forces measured are comparable with those measured at 0.2 µm/pass.

This work makes use of in-situ measurement techniques to measure the adhesions during rubs of differing test conditions to show that there is a statistically significant difference in wear behaviour at lower incursion rates. The use of in-situ thermal measurement combined with thermal analysis tools can then explain these differences by showing how the thermal energy added to the abradable at lower incursion rates can be conducted more effectively through the abradable.

Further work could be done to fill the gaps between testing completed here and real operation by investigating the impact of the elevated starting temperatures and backplate temperatures found in an engine.

CRediT authorship contribution statement

Aaron Baillieu: Writing – review & editing, Writing – original draft, Methodology, Investigation, Formal analysis, Data curation, Conceptualization. **Eldar Rahimov:** Methodology, Investigation, Data curation, Conceptualization. **Matthew Marshall:** Writing – review & editing, Supervision, Investigation, Conceptualization.

Funding

This research did not receive any specific grant from funding agencies in the public, commercial, or not-for-profit sectors.

Declaration of competing interest

The authors declare that they have no known competing financial interests or personal relationships that could have appeared to influence the work reported in this paper.

Data availability

Data will be made available on request.

References

[1] Oerlikon Metco, Material Product Data Sheet Aluminum Silicon Polymer Thermal Spray Powders, 2021.
[2] M.O. Borel, A.R. Nicoll, H.W. Schläpfer, R.K. Schmid, The wear mechanisms occurring in abradable seals of gas turbines, Surf. Coat. Technol. (1989).
[3] M. Watson, M. Marshall, Wear mechanisms at the blade tip seal interface, Wear 404–405 (2018 Jun) 176–193.
[4] J.F. Archard, Contact and rubbing of flat surfaces, J. Appl. Phys. 24 (8) (1953 Aug 1) 981–988.
[5] A. Gåård, N. Hallbäck, P. Krakhmalev, J. Bergström, Temperature effects on adhesive wear in dry sliding contacts, Wear 268 (7–8) (2010 Mar) 968–975.
[6] A. Gåård, P. Krakhmalev, J. Bergström, J. Hirvonen Grytzelius, H.M. Zhang, Experimental study of the relationship between temperature and adhesive forces for low-alloyed steel, stainless steel, and titanium using atomic force microscopy in ultrahigh vacuum, J. Appl. Phys. 103 (12) (2008 Jun 15).
[7] A. Baillieu, A. Parody, E. Rahimov, J. Garcia Panizo, M. Marshall, In situ measurements of thermal-mechanical wear in blade-abradable liner contacts, Proc Inst Mech Eng C J Mech Eng Sci (2023 Jul 18).
[8] Q. Agrapart, J.F. Brunel, Y. Desplanques, P. Dufrenoy, R. Mandard, A. Millecamps, An Energy Balance of Blade-Casing Interaction. 16th International Symposium on Transport Phenomena and Dynamics of Rotating Machinery (ISROMAC 2016), 2016 Apr.
[9] R. Bolot, J.L. Seichepine, F. Vucko, C. Coddet, D. Sporer, P. Fiala, et al., in: B. R. Marple, M.M. Hyland, Y.C. Lau, C.J. Li, R.S. Lima, G. Montavon (Eds.), Thermal Conductivity of AlSi/Polyester Abradable Coatings, 2008, pp. 1056–1061.
[10] M. Watson, M. Marshall, A novel image segmentation approach for microstructure modelling, Coatings 7 (10) (2017 Oct 4) 166.
[11] E. Rahimov, M. Watson, A. Hadjisoteriou, M. Marshall, Investigation of wear mechanisms in AlSi-polyester abradable - Ti(6Al4V) blade contacts using stroboscopic imaging, Wear 494–495 (2022 Apr) 204207.
[12] J. Stringer, M. Marshall, High speed wear testing of an abradable coating, Wear (2012).
[13] E. Rahimov, Investigation of Wear Mechanisms in Abradable-Blade Contacts, The University of Sheffield, 2022 [Sheffield].
[14] D. Jech, L. Čelko, P. Komarov, J. Ziegelheim, Z. Česánek, J. Schubert, The role of different atmospheric plasma spray parameters on microstructure of abradable AlSi-polyester coatings, Solid State Phenom. 270 (2017 Nov) 224–229.
[15] Z. Wu, Y. Zhang, Y. Xu, D. Jie, R.L. Jackson, Modeling of flash temperature for elastic sliding contact of single micro-asperity pair, J. Tribol. 146 (1) (2024 Jan 1).
[16] Y. Liu, R. Xu, J. Wang, S. Wan, L. Bai, Atomistic insight into flash temperature during friction, Int. Commun. Heat Mass Tran. 138 (2022 Nov) 106317.
[17] The MathWorks Inc, MATLAB Partial Differential Equation Toolbox, 2024.